Nat Hazards
DOI 10.1007/s11069-017-2918-z

ORIGINAL PAPER

Tsunami hazards in the Catalan Coast, a low-intensity seismic activity area

Ignacio Barranco[1,5] · Vicente Gracia[1,2] · Joan Pau Sierra[1,2] · Hector Perea[3,4] · Xavier Gironella[1,2]

Received: 23 June 2016 / Accepted: 8 May 2017

Abstract The potential impacts of tsunamis along the Catalan Coast (NW Mediterranean) are analysed using numerical modelling. The region is characterized by moderate to low seismic activity and by moderate- to low-magnitude earthquakes. However, the occurrence of historical strong earthquakes and the location of several active offshore faults in front of the coast suggest that the possibility of an earthquake-triggered tsunami is not negligible although of low probability. Up to five faults have been identified to generate tsunamis, being the highest associated possible seismic magnitudes of up to 7.6. Coastal flooding and port agitation are characterized using the Worst-case Credible Tsunami Scenario Analysis approach. The results show a multiple fault source contribution to tsunami hazard. The shelf dimensions and the existence of submerged canyons control the tsunami propagation. In wide shelves, waves travelling offshore may become trapped by refraction causing the wave energy to reach the coastline at some distance from the origin. The free surface water elevation increases at the head of the canyons due to the sharp depth gradients. The effects of potential tsunamis would be very harmful in low-lying coastal stretches, such as deltas, with a high population concentration, assets and infrastructures. The Ebro delta appears to

Electronic supplementary material The online version of this article (doi:10.1007/s11069-017-2918-z) contains supplementary material, which is available to authorized users.

✉ Vicente Gracia
vicente.gracia@upc.edu

[1] Laboratori d'Enginyeria Marítima, Universitat Politècnica de Catalunya BarcelonaTech, Jordi Girona 1-3, Mòdul D1, Campus Nord, 08003 Barcelona, Catalonia, Spain

[2] Centre Internacional d'Investigació dels Recursos Costaners (CIIRC), Jordi Girona 1-3, Mòdul D1, Campus Nord, 08003 Barcelona, Catalonia, Spain

[3] B-CSI, Institut de Ciències del Mar-CSIC, Psg. Marítim de la Barceloneta, 37-49, 08003 Barcelona, Spain

[4] GRD, Scripps Institution of Oceanography, University of California San Diego, La Jolla, CA 92093, USA

[5] Present Address: Department of Civil and Environmental Engineering, National University of Singapore, Singapore 117576, Singapore

Published online: 25 May 2017

be the most exposed coast, and about the 20% of the delta surface is prone to flooding due to its extremely low-lying nature. The activity at Barcelona port will be severely affected by inflow backflow current at the entrance of up to 2 m/s.

Keywords Tsunami hazards · Coastal impacts · Harbour impacts · Catalan Coast · Worst-case Credible Tsunami Scenario

1 Introduction

Tsunamis pose a very low-probability but potentially high-risk natural hazard, which may have catastrophic effects in coastal areas, damaging assets and even generating casualties. There are areas of intense seismic activity where this risk is evident and where authorities and population are aware of it. The 2004 tsunami in the Indian Ocean triggered the development and implementation of early warning systems (see Papadopoulos 2016 for a review), evacuation plans (UNESCO-IOC 2009; Scheer et al. 2012) and inundation maps. Nevertheless, there are other areas where although the seismic activity is frequent, it is of low intensity so that most earthquakes have not enough energy to generate tsunamis. In these areas, although strong earthquakes may have been recorded in the remote past, the perception of tsunami risk does not exist despite the fact that, although very low, the probability of having one of these events cannot be neglected. In particular, in densely populated regions, with extensive infrastructure and industrial facilities along the coast, the vulnerability to flooding by tsunamis is very high and therefore even low-probability or long-recurrence events need to be assessed.

About 300 descriptions of tsunami and similar phenomena are known for the Mediterranean Sea (Soloviev et al. 2000). The areas more struck by tsunamis are located in eastern and central regions, like the coast of insular Greece and the coast of southern Italy. Meanwhile, the western Mediterranean coast has also been historically impacted by tsunamis, but the generated waves were more moderate or less documented than the ones reported in the eastern part of this region (Gailler et al. 2013). Besides this, in western Mediterranean some tsunamis related to earthquakes with epicentres near the coast of Algeria (Tinti et al. 2005a; Kherroubi et al. 2009) or the French Riviera (Scotti et al. 2004) have been generated.

Most of the earthquake-induced tsunami studies in the Mediterranean have focused on the reconstruction of specific past events with the main purpose of constraining the earthquake source parameters (e.g. Tinti and Piatanesi 1996; Piatanesi and Tinti 1998, 2002; El-Sayed et al. 2000; Alasset et al. 2006; Gutscher et al. 2006). Others have used hypothetical or inferred earthquake source parameters for constructing tsunami scenarios (e.g. Pelinovsky et al. 2002; Tinti et al. 2005a; Álvarez-Gómez et al. 2011). There are also tsunami simulations oriented to both tsunami risk estimation and forecasting. In this regard, tsunami hazard in a certain area can be computed adopting different approaches like the Worst-case Credible Tsunami Scenario Analysis (WCTSA) or the Probabilistic Tsunami Hazard Analysis (PTHA). According to Tonini et al. (2011), PTHA seems more exhaustive and more informative than WCTSA, but PTHA requires more input data and computational effort and its use in case of lack of data may be questionable. Examples of application of WCTSA are Tinti et al. (2005a); Titov et al. (2005); Lorito et al. (2008);

Tonini et al. (2011). The PTHA approach has been used by Tinti et al. (2005b); Geist and Parsons (2006); Grilli et al. (2009); and Grezio et al. (2010, 2012) among others.

The Spanish Mediterranean border has a moderate to low occurrence and magnitude/intensity seismic activity (Papadopoulos et al. 2014). However, since the 1960 s, the coast has experienced an intense urban development shifting most of the population to coastal areas. As a consequence, the occupation of the littoral enormously increased and numerous tourist resorts, houses, marinas and other infrastructures were built. Therefore, the assets and population exposed to eventual tsunami hazards are greater than ever and, for this reason, Spain is considered a country with a higher tsunami risk (Álvarez-Gómez et al. 2011).

There are also a number of studies about tsunami propagation and impact on Spanish Mediterranean coasts. Wang and Liu (2005) performed a numerical investigation to evaluate the accuracy of various suggested fault plane mechanisms for the earthquake and tsunami of Boumerdes–Zemmouri (Algeria) occurred in 2003, calibrating the model with data of tide gauges located in the Balearic Islands. Alasset et al. (2006) studied the same event, testing different seismic sources and modelling the tsunami initiation and propagation and comparing the results with tide gauge records in order to determine the source of the tsunami. Roger and Hébert (2008) made a numerical simulation of the 1856 Djijelli (Algeria) tsunami and its impact on Balearic Islands, in particular on Mallorca and Menorca Islands. Yelles Chaouche et al. (2009) simulated also this tsunami analysing its effects on Balearic Islands and the city of Djijelli. Álvarez-Gómez et al. (2010, 2011) analysed the impact of tsunamis induced by north Algerian seismic sources on the Island of Mallorca and studied the tsunami hazard at the Mediterranean Spanish coast. All these studies have two features in common: they analyse tsunami propagation generated in a source located in a particular region of the western Mediterranean (mainly Algeria), and they study the impact of tsunamis on a particular stretch of the Spanish Mediterranean coast (mainly the Balearic Islands).

The Catalan Coast (Spanish Mediterranean) is an area of frequent seismic activity although with low intensity. Even although this area can be considered relatively safe from tsunamis generated in North Africa, geologic studies (Perea et al. 2006, 2012) showed that a number of faults located in the Catalano-Balearic Sea have potentiality to produce earthquakes with magnitudes larger than 7 and, thus, could be responsible for future unexpected tsunamis in the zone.

Therefore, the aim of this paper is to perform a study of the tsunami hazard in the Catalan Coast, taking into account the features of the faults located in front of this coast. The study focuses on beaches and coastal infrastructures, with special emphasis on coastal flooding and port agitation. The paper is structured as follows: in Sect. 2, the study area is described, in particular its geological and seismological features. The methodology and data used are presented in Sect. 3. In Sect. 4, the obtained results are displayed and discussed. Finally, in Sect. 5, the main conclusions are presented.

2 Study area

2.1 Site description

The Catalan Coast (Fig. 1) is located in the NW Mediterranean border and limited by the Gulf of Lion (France) to the north and the Ebro Delta (Spain) to the south. This coastal

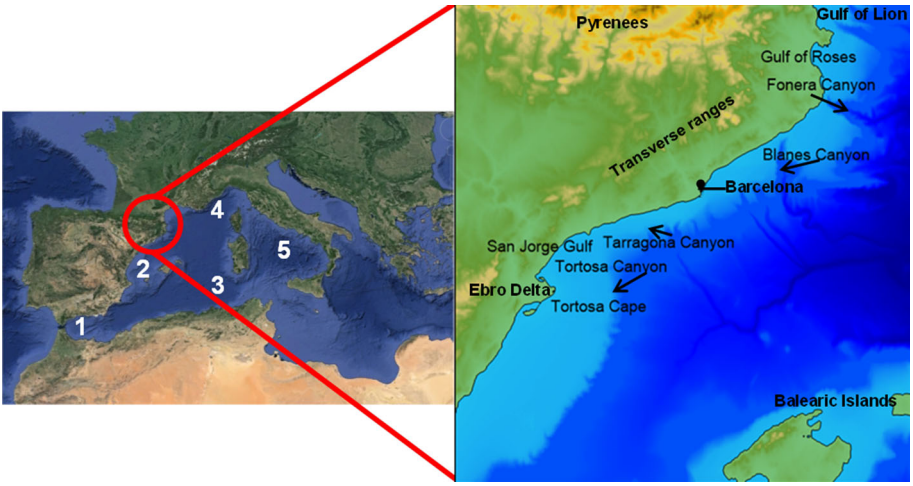

Fig. 1 Location of the Catalan Coast and some physical features of the area. In *left panel*, *1* Alboran Sea, *2* Valencia trough, *3* Algerian basin, *4* Ligurian-Provençal basin, *5* Tyrrhenian basin

stretch has an approximate length of 700 km, and its continental margin is crossed by several submarine canyons of different evolutionary history (Canals et al. 2004).

The coastal fringe presents almost all types of littoral environments. The main morphological features are (from south to north): (1) the Ebro Delta unit (a 50-km sandy fringe) and the low-lying beaches of Costa Daurada, (2) the straight segmented relatively coarse beaches at the centre (represented by the Barcelona–Maresme system), and (3) the pocket beaches and cliffs near the French border (Costa Brava). The strong anthropogenic pressure and the economic activity developed in the area during the last 30 years have created a very fragmented coastal landscape as a result of the marine facilities and different coastal protection interventions. Moreover, urban sandy beaches usually border the coastal backside with a seafront promenade and infrastructures such as streets, roads, railways or houses. Few coastal stretches remain pristine or have a low human imprint. The Ebro delta at the south and the Gulf of Roses at the north are examples of these low-lying natural environments.

The central part of the coast is under the influence of the Barcelona metropolitan area and contains most of the marinas and urban settlements. The main economical attraction points are the harbour and airport of Barcelona. The activities performed by the Port of Barcelona—ship, logistics and intermodal transport services—directly and indirectly generate Gross Value Added (GVA) for the economy to the tune of 2.291 billion €, which represents the 1.4% of Catalonia's total GVA. The direct and indirect employment associated with the harbour represents the 0.9% of Catalonia's job market (BPA 2015). The Barcelona airport, located three kilometres from the Port of Barcelona, is the second biggest in Spain. In 2015 it was the 10th European airport in passenger traffic.

As can be seen, the high concentration of population, assets and infrastructures makes the Catalan Coast particularly vulnerable to hazards coming from the sea-like wave storms or tsunamis.

2.2 Geological and seismological settings

The opening of the Atlantic Ocean and the collision between African and Eurasian plates have controlled the geodynamics of the Iberian microplate. During the Neogene, an extensional back-arc process took place in the western Mediterranean due to the subduction of Africa beneath Eurasia (e.g. Malinverno and Ryan 1986; Royden 1993; Gueguen et al. 1998; Doglioni et al. 1999; Jolivet et al. 1999; Gelabert et al. 2002; Rosenbaum et al. 2002; van Hinsbergen et al. 2014; Chertova et al. 2014). As a consequence, a number of extensional basins were formed (the València Trough, the Alboran Sea, the Ligurian-Provençal, the Algerian and the Tyrrhenian basins). Specifically, the Valencia through basin is a NE–SW-trending basin with a wedge shape opening towards the NE and being limited to the NW by the Catalan and Valencia coasts and to the SE by the Balearic Islands promontory. Two tectonic phases have been defined in the evolution of the Valencia trough basin since the Neogene (Roca and Guimerà 1992; Roca 1996, 2001; Roca et al. 1999): (a) a rifting phase that lasted from the late Oligocene to middle Miocene and during which a NE–SW-trending rift system with a total extension of 7.1 km developed; and (b) a thermal subsidence phase characterized by moderate tectonic activity mainly localized along the borders of the basin and by a total extension of 4.1 km since the middle Miocene to the present.

The geological structure in the north western margin of the Valencia trough basin is controlled by several extensional faults forming a horst and graben system. The main faults are listric, dip 60°, have normal dip slip, branch in a common detachment level at approximately 15 km depth, accumulate kilometric displacements and have produced a considerable crustal thinning on the axis of the basin (Roca and Guimerà 1992; Roca 1996, 2001; Sàbat et al. 1996; Roca et al. 1999; Vergés and Sàbat 1999; Gaspar-Escribano 2004). Although these faults are under low strain rates, different studies have proposed that some of them, onshore and offshore, are still active with slip rates ranging between 0.1 and 0.01 mm/yr and capable of producing large earthquakes ($M > 6$) with mean recurrence intervals between 10^3 and 10^5 years (Masana et al. 2001a, b; Perea et al. 2003, 2006, 2012; Perea 2009).

The instrumental seismicity around the Catalan Coast is low and characterized by earthquakes of low to moderate magnitude (maximum reached $M_w = 5.1$) (Olivera et al. 1992; Perea et al. 2006, 2012). Moreover, the earthquakes are described as shallow regarding that more than 90% of the events are located between the surface and 15–20 km depth, which may correspond to the thickness of the seismogenic crust. Accordingly to this and in agreement with the location of the common detachment level, the fault rupture planes used in the tsunami modelling do not surpass the 15 km depth. Geographically, the highest earthquake density is localized in the Pyrenees and the Transverse ranges, whereas the lowest density is observed across the Catalan and Valencia coasts. Despite the low-intensity seismic activity, some large earthquakes have occurred in the past, such as those of the Catalan seismic crisis in 1427 and 1428 (earthquakes of Amer, Olot and Camprodon with intensities—MCS scale—of VIII, VIII and IX, respectively) (Olivera et al. 2006; Perea 2009) or as those deduced from palaeo-seismological studies (Masana et al. 2001a, b; Perea et al. 2003). Accordingly, it could not rule out the possibility of occurrence of a future large earthquake in the area and the important economic and social consequences it could have, considering that the area is densely populated, very industrialized and with important infrastructures (e.g. nuclear power plants or harbours).

3 Materials and methods

3.1 Model description

The most extended models to simulate tsunami propagation are based on the nonlinear shallow-water equations, like MOST (Titov and Sinolakis 1998), COMCOT (Liu et al. 1994, 1995; Wang and Liu 2006), TSUNAMI2 (Imamura 1996) or UBO-TSUFD (Tinti et al. 2006; Argnani et al. 2012) or on Boussinesq equations, like FUNWAVE (Wei and Kirby 1995; Chen et al. 2000; Kennedy et al. 2000) or COULWAVE (Lynett and Liu 2002, 2004; Lynett et al. 2002; Kim et al. 2009). In this paper, the COMCOT model has been used to analyse the tsunami-related hazards along the Catalan Coast. The model simulates the entire lifespan of a tsunami, including the generation, propagation and run-up. It has been previously used to reproduce recent recorded tsunamis like the event of May 2003 in Algeria (Wang and Liu 2005) and the episode in the Indian Ocean in 2004 (Wang and Liu 2006).

The tsunami generation mechanism in the model assumes that the initial water displacement generated by the earthquake is identical to the vertical displacement of seabed induced by the ground motion, which is determined using the expressions proposed by Mansinha and Smylie (1971) and Okada (1985). This hypothesis is reasonable because the rupture typically has duration of few minutes, which can be considered instantaneous comparing to the timescale of tsunami propagation. Since the WCSTA approach is used, a duration enough long to reach the maximum tsunami elevation is assumed.

COMCOT adopts a modified leapfrog finite-difference scheme to solve (both linear and nonlinear) shallow-water equations (Liu et al. 1994, 1995) in both Spherical and Cartesian coordinates and uses a nested grid system that allows to save computational time, with a detailed mesh in the coastal region and a broader mesh in deepwater areas where a more precise mesh is not necessary. Finally, to simulate the wave run-up, COMCOT uses a moving boundary scheme.

3.2 Tsunami impact assessment

Tsunami scenarios are commonly used to determine the vulnerability of a specific coastal area; their results are used to define guidelines in policy planning. To analyse the Catalan Coast exposition to tsunamis, the WCTSA has been used. Similar approaches can be found in the literature to study the tsunami hazard in different areas (Tinti et al. 2005a; Okal and Synolakis 2008; Lorito et al. 2008; Tonini et al. 2011; Pagnoni et al. 2015; Armigliato et al. 2015).

The WCTSA can be described as a three-step framework: (1) the source identification; (2) the generation and propagation; and (3) the building of a unique aggregated scenario. The construction of the worst-case scenario is obtained by generating and propagating tsunamis triggered by the offshore faults with their associated major earthquakes. The parameters necessary to characterize the seafloor displacements responsible of these earthquakes are: (1) the epicentre, (2) the focal depth, (3) the fault length, (4) the fault width, (5) the strike, (6) the dip, (7) the slip and (8) the rake. The elastic fault model has been used in the generation mechanism. Thus, the model assumes an idealized rectangular plane as the interface between two colliding plates, and the fault motion takes place on this plane and the water surface will follow the seafloor uplift.

On the other hand, shallow-water tsunami wave propagation is strongly influenced by the existing bottom morphology (Iglesias et al. 2014). Therefore, to obtain realistic results, detailed topo-bathymetric information, describing relevant morphology details, is required. The fault parameters and topo-bathymetry data used in this study are described in Sect. 3.3.

To study the potential impacts of tsunamis in the Catalan Coast, the offshore effects and the inland repercussions of these waves have been analysed. The offshore effects have been described for every case by the wave estimated times of arrival to the coast and the maximum water surface elevations achieved. The maximum water surface elevations registered during the events are plotted in maximum free surface elevation (FSE) maps, which indicate the hazard distribution in worst-case scenarios studies.

Coastal flooding and port agitation are the main hazardous effects provoked by tsunami on the coast, although not all the tsunamis are strong enough to cause them. In this study, the effects of the most powerful waves generated on the most affected areas have been analysed through flooding maps which show the areas inundated during the events. These maps are used to identify areas most vulnerable to inundation and for land-use planning. Nevertheless, these maps must be interpreted with caution because maximum/minimum FSEs may occur with significant time lag, and therefore, they are not representative of the maximum agitation, although they indicate the minimum and maximum levels reached during the event. On the other hand, to characterize Barcelona Port agitation, maximum and minimum FSE maps have been used, which show the complete FSE range during the events. In addition, flow maps showing the water velocities' distribution within the port boundaries have been plotted because current velocity and wave height are the two variables primarily used to define port operability.

3.3 Data and modelling strategy

The required fault information in the area has been obtained from Perea et al. (2006, 2012). These authors estimated the maximum magnitude (Mw) earthquake on each fault assuming that the mapped length of each fault corresponds to the maximum surface rupture length that an earthquake could produce and using available empirical relationships for normal faults (Wells and Coppersmith 1994). On the offshore, since there is no geomorphologic evidence of these faults on the seafloor, industrial reflection profiles were used to map their length (Roca 1996, 2001; Roca and Guimerà 1992) and to determine their present activity (Perea et al. 2006, 2012). Usually, in this type of profiles, the vertical resolution does not allow to detect small fault offsets in shallow reflectors, as those expected in areas characterized by slow slip-rate faults. However, considering that the area has been affected by a thermal subsidence (Roca and Guimerà 1992; Roca 1996, 2001; Roca et al. 1999) and the stress field is similar to the one that resulted in the formation of the faults (Perea et al. 2006, 2012), it has been assumed that the faults offsetting the shallow reflectors corresponding to the Plio-Quaternary units, as the ones studied here, are still active and may produce large earthquakes in the future.

The worst-case tsunami scenario has been built by analysing the wave characteristics triggered by five offshore faults with a seismic magnitude greater than 6.9 (Fig. 2). Other unknown necessary data have been selected as follows:

- Epicentre latitude and longitude: the epicentre has been placed in the centre of the mapped active fault planes.
- Focal depth: since earthquakes at this area usually occur at depths between 5 km and 15 km, the middle value (10 km) has been used for all the cases.

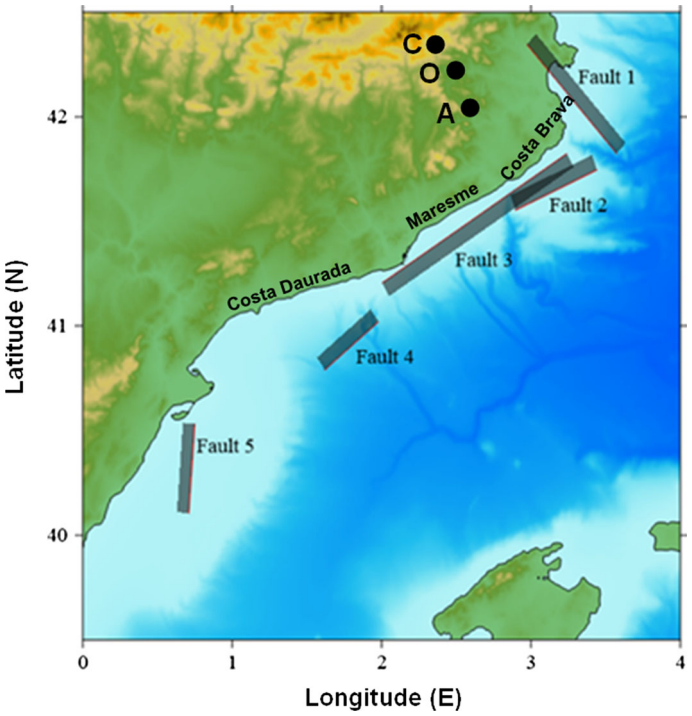

Fig. 2 The Gulf of Roses fault (*Fault 1*), Blanes fault (*Fault 2*), Barcelona fault (*Fault 3*), Salou fault (*Fault 4*) and fault of the Amposta basin (*Fault 5*). *Red lines* represent the intersection of the fault plane with the seafloor and the *grey transparent rectangles* the projection of the fault plane on the seafloor. The location of past large earthquakes is also shown (*A* Amer, *O* Olot, *C* Camprodón)

- Slip (dislocation) has been obtained through the seismic moment equation

$$M = \mu A D.$$

where M is the seismic moment, μ is the rock rigidity, A is the fault area, and D is the average dislocation. For the rock rigidity, due to the lack of data, a close-to-average typical value of 32 GPa has been assumed, which is similar to that used for many authors, as for example Lay et al. (2005) for the Sumatra–Andaman Trench. Since rigidity varies quite a bit from region to region, we keep in mind that the actual values in the studied area could be different and, therefore, also the results, which can be considered preliminary.

To calculate the M corresponding to the maximum earthquake, we have used the given Mw and the Hanks and Kanamori (1979) relation. The A has been estimated using the mapped surface length of the fault and the width of the fault plane, obtained considering that the fault dips 60° and extends from the seafloor up to 15 km depth (Table 1). The equation is used in an inverse manner, that is, known the seismic moment of a Worst-case Credible Tsunami Scenario (according to Perea et al. 2006, 2012), the associated dislocation is found. In addition, a uniform slip distribution on the fault is assumed since it corresponds to the WCTSA, although heterogeneities could lead to different results.

Table 1 Seismic parameters associated with the five-fault worst-case scenario

Fault name	Fault 1 Roses	Fault 2 Blanes	Fault 3 Barcelona	Fault 4 Salou	Fault 5 Amposta
Epicentre latitude (°)	42.11	41.685	41.483	41.685	40.321
Epicentre longitude (°)	3.304	3.153	2.645	3.153	0.69
Focal depth (km)	10	10	10	10	10
Length (km)	76.1	50.1	123.3	50.1	47.6
Width (km)	17.3	17.3	17.3	17.3	17.3
Strike θ (°)	140	245	56	245	184
Dip δ (°)	60	60	60	60	60
Slip (m)	2.66	2.03	4.63	1.77	2.13
Rake λ (°)	−90	−90	−90	−90	−90
Seismic magnitude	7.3	7.1	7.6	7.0	7.1

With respect to the rake, since the faults in the area have been characterized as normal faults (Perea et al. 2006, 2012), an angle of −90° has been selected because it gives the maximum movement in the vertical direction, being the most hazardous expected case. Table 1 shows a summary of the seismic parameters associated with the five-fault worst-case scenario earthquake (Perea et al. 2006, 2012).

The model setup is structured in a sequence of nested grids in four different levels (Fig. 3). The first level (grid A) covers the northeast Iberian Peninsula Coast and part of the Balearic Islands. There are three grids in the second level (B1, B2 and B3) covering the northern, central and southern parts of the Catalan Coast. These two levels have been used to carry out the WCTSA. Once the hazard along the Catalan Coast has been assessed, the third and four levels have been built where the analysis showed a higher hazard, to make more precise studies, including inundation analysis. Thus, the third-level grids contain the areas studied in detail: Gulf of Roses (C1), Barcelona and surroundings (C2) and Ebro Delta (C3). The fourth level (D) includes the Barcelona Harbour. The different grids have been integrated into a nested spherical coordinate system, and all use nonlinear equations and the same Manning's roughness parameter 0.013. Grid size ratios between 4 and 5 have been used in the different levels. Table 2 shows the different grid parameters used in the study.

The necessary topographic and bathymetric data for the above-described model strategy have been obtained from the following databases:

- The *GEBCO_2014 Grid*, with a resolution of 30". It has been used in the two coarser grids, where the level of detail needed is not as demanding.
- The *EMODnet Bathymetry* from the European Marine Observation and Data Network, generated from bathymetric survey datasets and composite digital terrain models (DTM). It has a resolution of 0.125' and has been used for the finer grids. It has to be complemented with topography data for inundation studies.
- *DTM* from the *Institut Cartogràfic de Catalunya*, with a horizontal resolution of 15 m and altimetric accuracy of 0.9 m (value of the root-mean-square error). It has been used to complement the EMODnet bathymetry.

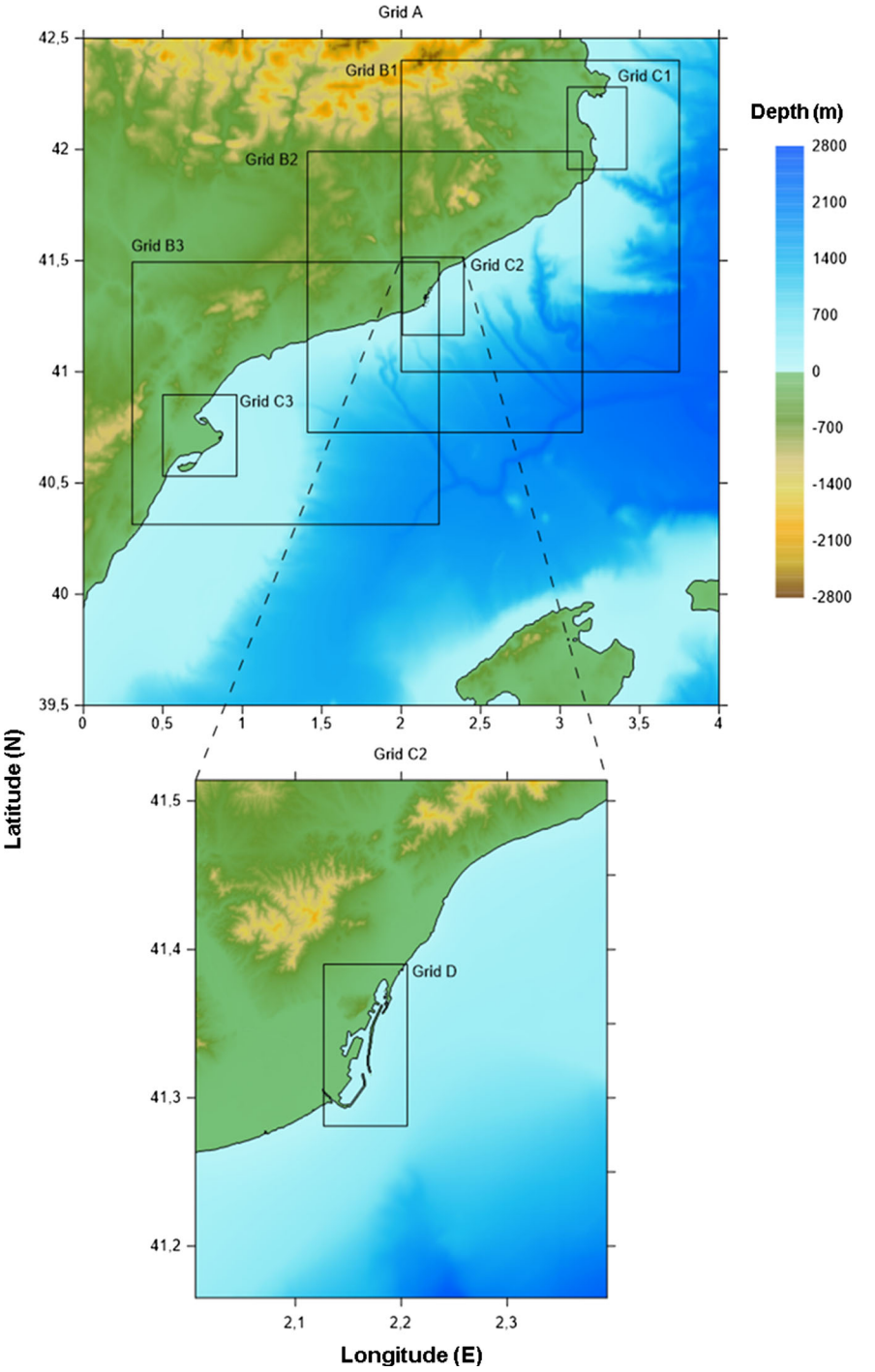

Fig. 3 Catalan Coast nested grids. *Upper map* corresponds to Grid A, where Grids B and C are indicated. *Lower map* is a detail of the C2 upper one where Grid D is situated. Water depths are in *positive numbers*

Table 2 Grid characteristics used in the analysis

Grid	Level	South boundary (°)	North boundary (°)	West boundary (°)	East boundary (°)	Grid resolution (minutes)	Number of nodes
Grid A	1	39.5	42.5	0	4	1	241 × 181
Grid B1	2	41	42.4	2	3.75	0.25	421 × 337
Grid B2	2	40.72708	41.98958	1.410417	3.139584	0.25	416 × 304
Grid B3	2	40.3126	41.4926	0.3075	2.2375	0.25	460 × 280
Grid C1	3	41.9091	42.27942	3.0456	3.41925	0.05	459 × 454
Grid C2	3	41.16499	41.51416	2.00583	2.39416	0.05	467 × 420
Grid C3	3	40.53	40.8969	0.5	0.9653	0.05	559 × 441
Grid D	4	41.28094	41.3899	2.12771	2.205729	0.0125	380 × 524

- *Barcelona Port Bathymetry* provided by the port authority with a resolution of 23 m has been used to study this singular infrastructure.

4 Results and discussion

4.1 The Gulf of Roses fault

The fault is placed in the Gulf of Roses, a low-lying coast with urbanized areas and several campsites on the seaside, as well as the Empordà Marshes Natural Park (Figs. 2 and 4). The fault is perpendicular to the general Catalan coastline, being partially inland in its northwest end. Its maximum associated earthquake magnitude is M_w 7.3. Its initial movement causes a maximum FSE of 0.37 m in the coastal side and a maximum 1.32 m free surface depression offshore.

The generated tsunami (Fig. SM1 in the Supplementary Material) propagates in two fronts: a trough–crest system travelling towards the south and a crest–trough unit moving towards the north. The results indicate a complex tsunami circulation pattern with important coastal reflections at the Montgrí cliffs and the shelf and submarine canyons. The existing relative wide shelf induces the trapping of the southern wave front in such a way that it returns to L'Estartit after approximately 10 min after its generation inducing the highest FSE in the area. La Fonera canyon appears to be a morphological barrier for the tsunami propagation concentrating the wave energy in the canyon head (close to the coast) and permitting its travel towards the south. About 15 min after the earthquake, there is an interaction between reflected waves and the trapped refracted front causing important FSE at the Gulf of Roses coastline. The results show the trap effect of the Gulf of Roses for also the reflected–refracted waves from the northern front. As a result of this, a maximum in the FSE is generated in the area.

The maximum FSE map (Fig. 4) shows the highest tsunami affectations between the enclosed coastal stretches of the Gulf of Roses and L'Estartit although it is observed up to 100 km southwards. The maximum modelled FSE is 6.4 m. A significant flooding is observed in both areas severely affecting the inland. The total flooded area during the event is 33.8 km^2, and the water reaches 2.5 km inland (Fig. 4). The maximum run-up is 5.36 m. The village of Roses, the highly urbanized marinas of Empuriabrava and Santa Margarida,

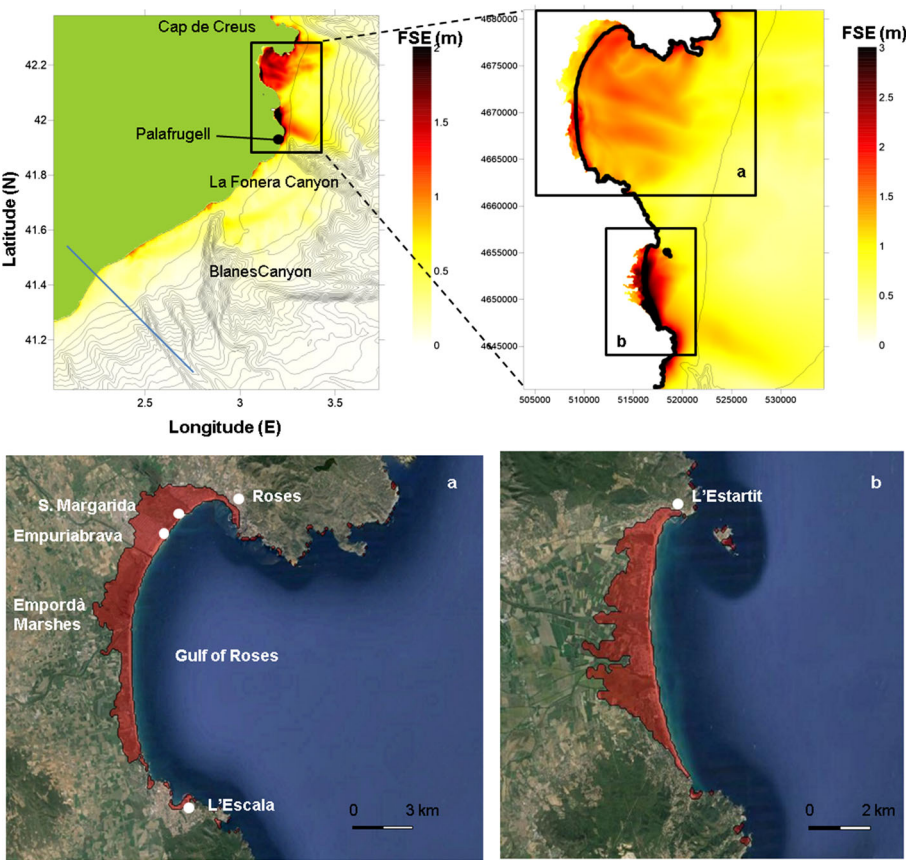

Fig. 4 *Upper panels* Maximum water elevation for the Gulf of Roses fault scenario. Bathymetry contour lines are plotted every 100 m. *Lower panels* Flooded areas (in *red*) for the same scenario in the Gulf of Roses (*left*) and in L'Estartit (*right*) areas

the Baix Empordà Marshes Natural Park and the existing coastal holiday resorts and campsites are the main affected infrastructures at the north. Given that the fault is entering in the onshore, the displacement on the fault plane in this area could produce some subsidence increasing the possible flooded area. Thus, the obtained values should be considered as minimum. A similar landscape is observed at L'Estartit, being the village, the existing farmlands and small resorts also affected by the tsunami. The fault is able to significantly affect up to 16 campsites.

The topography influence in the inundation process is evident since the flooding is greater in areas near rivers mouths, marshes and canals, where the topography is low-lying or even below the sea surface. The inundations would take place when the maximum wave crest hits the coast. The Gulf of Roses shore is reached 20 min after the earthquake; meanwhile, L'Estartit area is reached before, 15 min after the event. The arrival times derived from the simulations were too short and hardly would allow a warning notice and evacuation ordered by the authorities. For this reason, self-evacuation based on natural signs such as strong ground shaking should be exercised.

4.2 The Blanes fault

The Blanes fault (Figs. 2 and 5) is located between La Fonera Canyon and Blanes Canyon, and it slides towards the coast. Its maximum earthquake magnitude is M_w 7.1 and causes an initial maximum uplift of 0.3 and 1.1 m of maximum depression. The generated wave crests propagate initially parallel to the coast (see Fig. SM2 at Suppl. Mat.). The Blanes canyon at the south and La Fonera canyon at the north limit the alongshore front growth concentrating the energy on the coast. The highest FSE is reached between minutes 15 and 20 with a maximum value of up to 3.2 m. The maximum FSE plot for Blanes fault scenario shows how the higher water elevations are concentrated in front of Palamós. In the surrounding areas, there are some significant surface elevations, but they do not produce remarkable flooding. The low maximum FSE together with the high-lying topography in the area prevents significant inundation, and therefore, the hazard associated with this fault is expected to be low.

4.3 Barcelona fault

The Barcelona fault is located 10 km offshore from the coastline and parallel to it (Figs. 2 and 6). It is 123 km long and the longest fault considered in this study. It also has the largest earthquake magnitude (M_w 7.6) and the largest slip (4.63 m). Similarly to the Gulf of Roses fault, Barcelona fault slides seawards. The initial displacement produces a maximum free surface depression of 2.2 m and a maximum FSE of 0.8 m.

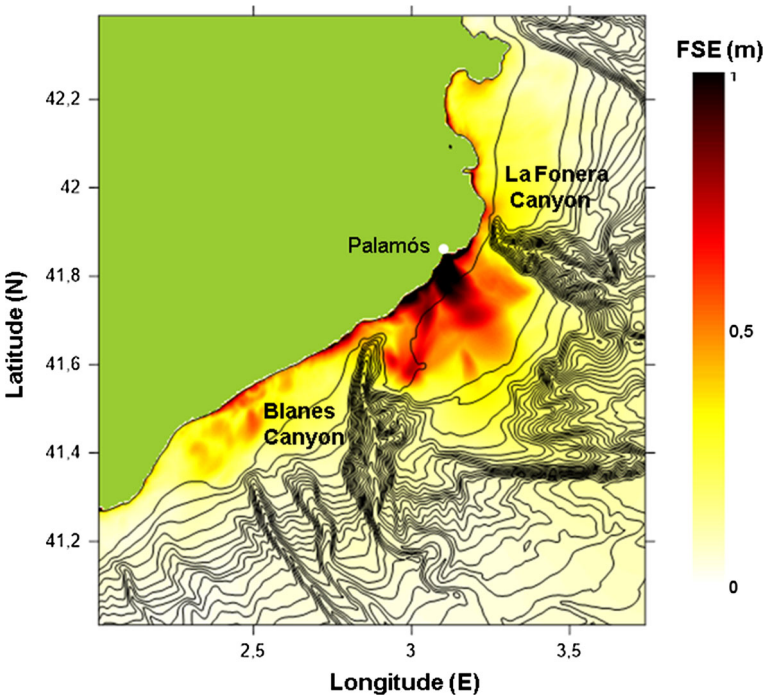

Fig. 5 Maximum water elevation for the Blanes fault scenario. Bathymetry contour lines every 100 m

The results show that the most important tsunami activity is developed within the first 50 min (Fig. SM3 at Suppl. Mat.). The coastline is affected by the initial disturbance because of the short distance between them. A wave crest can be observed in front of the coast 10 min after the earthquake. At minute 20, the crest has reached the entire coast, and at the same time, the offshore wave propagates faster towards the Balearic Islands because of the deeper bathymetry of the basin. The wave trough arrives to the coast of the Balearic Islands (180 km eastwards) at minute 30 and to the Ebro Delta (150 km southwards) at minute 40 after the earthquake.

The generated waves hit first Blanes at the north and the Barcelona Port at the south. In the first case, the Blanes canyon acts as coastal attractor, as the Fonera canyon in the Gulf of Roses fault scenario, by increasing the wave celerity through the canyon and refracting it. Nevertheless, this effect is very local and of low magnitude due to the limited width of the canyon and the short distance. In the case of Barcelona Port, this early arrival is due to its proximity to the fault. The small canyons located in front of Mataró at the north may also influence the wave propagation too, causing the highest wave concentrations in

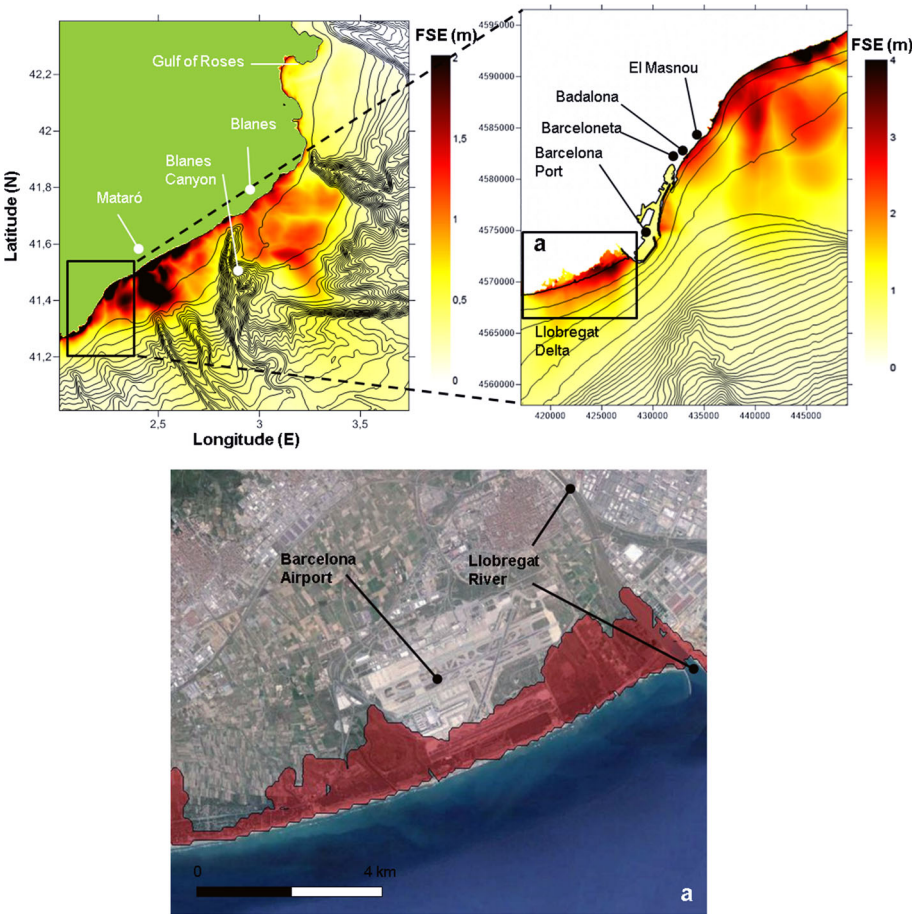

Fig. 6 Maximum water elevation for the Barcelona fault scenario (*upper panels*) with bathymetry contour lines every 100 m (*left*) and 20 m (*right*). *Lower panel* Flooded area in red in the Barcelona airport area

Mataró area (Fig. 6). The largest concentration of tsunami energy there is due to the "wave guide" effect of the much shallower ridge between the two neighbouring canyons, since waves travelling into the two canyons are refracted towards the shallower depth area between the two canyons, focusing more energy to Mataró. The maximum FSE registered is 5.5 m.

A significant flooding can be observed at the south of the Barcelona Port partially affecting the airport facilities and the existing campsites. The water moves through the Llobregat river mouth and advances to the southwest side of the airport up to 2 km inland. The total inundated area is 8.5 km^2. The low-lying nature of the region, situated in the Llobregat delta, totally controls the flooding. Thus, areas with higher FSE (mainly at the north of Barcelona) will not experience such flooding because the land infrastructures also have a high topographic level (greater than 3.5 m). As an example, the railroad at El Masnou although is located at less than 100 m from the shoreline is build at datum +4 m above the mean water level and acts as a coastal defence against flooding. The maximum run-up is 4.38 m.

Figure 7 shows the maximum and minimum water elevations recorded at Barcelona port during the event. The breakwater crown elevation, up to +12.5 m above the mean water level, is significantly higher than the obtained FSE (less than 2 m), and consequently, overtopping during the event is not expected. Inside the harbour, there is almost uniform maximum and minimum elevation distribution of about 1 m (positive and negative).

The tsunami propagation inside the port is shown in Fig. 8. The simulation starts with steady flow conditions. The tsunami enters first in the southern harbour mouth. An intense offshore current is developed at the south of up to 2 m/s associated with the through pass. A similar pattern less intense (of up to 1 m/s) is observed at the north 2 min later. A second wave front hits the harbour following the same direction of propagation although in this case the wave crest is big enough to generate an inflow current of similar magnitude and an

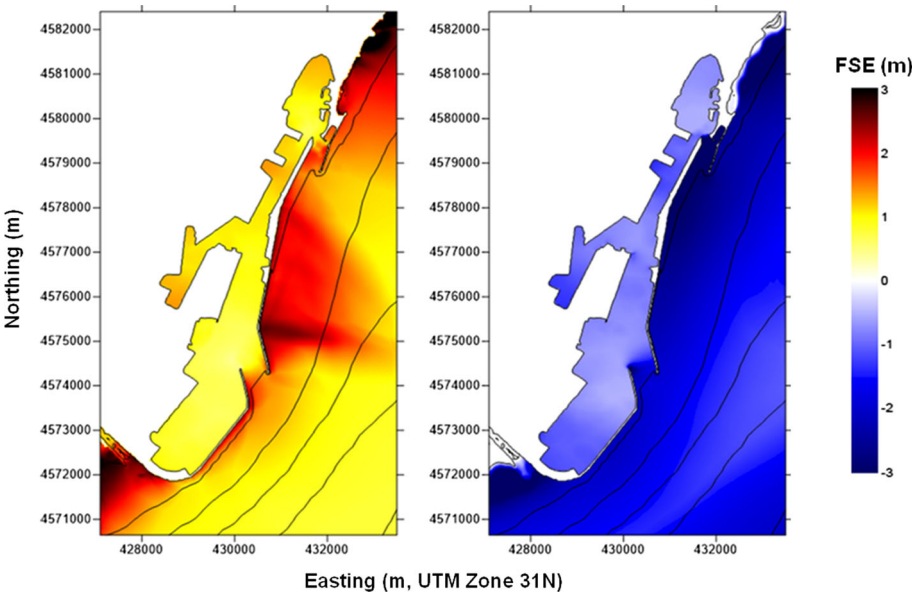

Fig. 7 Maximum and minimum free surface elevation in the Barcelona Port for the Barcelona fault scenario. Bathymetry contour lines every 20 m

eddy. Finally, around minute 30 a well-developed wave front from the north impacts the harbour affecting the southern mouth mainly due to its more exposed orientation and big dimensions.

The flow velocities and the wave heights registered during the event within the harbour reach values of up to 1 m/s and 1 m. The developed inside hydrodynamics reflects the differences in the harbour geometry. The southern basin has the largest dimensions, with a wider entrance of about 370 m at 16 m depth, whereas at the north, the second entrance is narrow (145 m) and shallow (11 m). Because of that, a more clear current field and eddy is developed and propagated at the south, whereas at the north, the tsunami affects immediately the entire area.

The tsunami has repercussions on the entire harbour activities making the manoeuvring or anchoring hazardous. According to the regulations of the Spanish Harbour Authority (Puertos del Estado, ROM 3.1-99), the conditions reached (wave height and flow velocities) will be large enough to stop most of the activity.

4.4 Salou fault

The Salou fault (Fig. 2) is situated between Tarragona and Tortosa canyons. It has the smallest maximum credible earthquake magnitude Mw 7 among the studied faults and the smaller slip 1.77 m. The initial movement causes a 0.3 m maximum water elevation offshore and 0.9 m free surface depression towards the coast.

The wave development (Fig. SM4 of Suppl. Mat.), unlike the previous cases, propagates without being affected by coastal reflections. The fault location, at the border of a wide

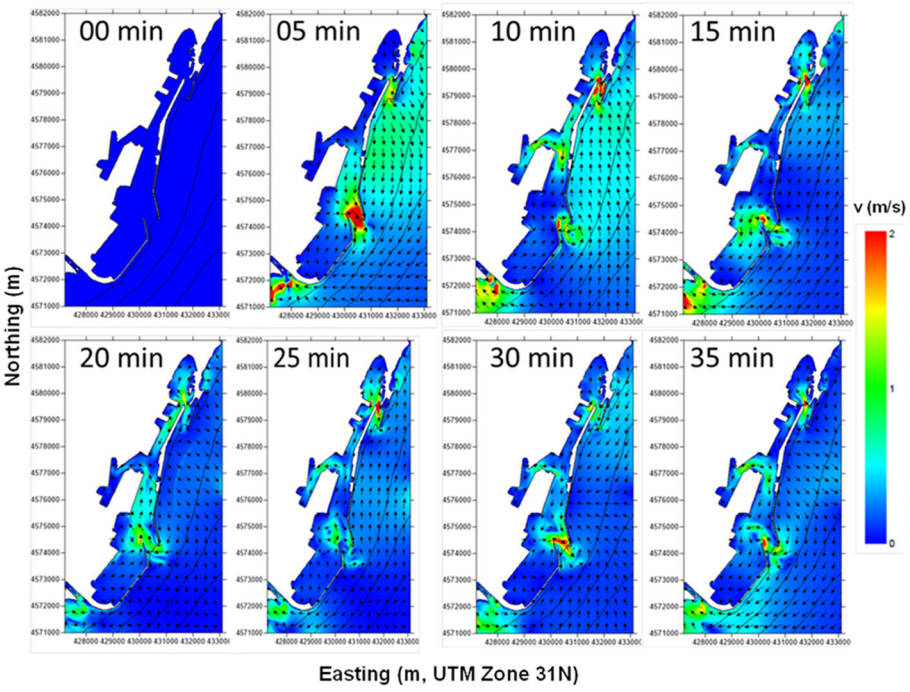

Fig. 8 Tsunami-induced current velocities inside the Barcelona Port for the Barcelona fault scenario. Flow velocities v (m/s). Bathymetry *contour lines* every 20 m

shelf, leads to steady wave propagation. The trough reaches the coast at minute 15. The continental shelf morphology appears to be an important element controlling the tsunami propagation. The Ebro delta continental shelf, at the south of the fault, is wider and presents a steeper continental slope with respect to the area located to the north of the fault. For this reason, the wave propagation at the south is slower and the Ebro delta coast is reached after 25 min although with a small FSE. The maximum FSE is presented in Fig. 9. The wave energy focuses on the coasts around Vilanova i la Geltrú and Torredembarra. The results indicate that the Tarragona Canyon influences the wave propagation as in previous cases although with less intensity. The maximum FSE recorded is 1.8 m, and significant flooded areas cannot be appreciated.

4.5 Fault of the Amposta basin

The fault of the Amposta basin (Fig. 3) is located at the south of the Ebro Delta; it has a north–south direction and slides to the coast. Its maximum earthquake magnitude is M_w 7.1 and generates a 0.3 m maximum initial offshore FSE and a 1.1 m maximum onshore depression. Figure SM5 (Suppl. Mat.) shows the tsunami development. The fault displacement generates two trough–crest fronts propagating towards the south and north, respectively. The first system arrives to the southern coast after 20 min and generates a reflected wave that propagates offshore and remains in the shelf. The second front propagates to Sant Jordi Gulf and is trapped in the shelf by refraction causing a refracted wave front to reach the Ebro delta. Trapped reflected waves have been previously discussed by Camfield (1982, 1988) and in the Shore Protection Manual (Shore Protection Manual (SPM) 1984). Both wave fronts of the reflected crest from the south and the trapped onshore propagated front from the north interact around minute 50 producing the highest FSE of the event along the southern hemidelta.

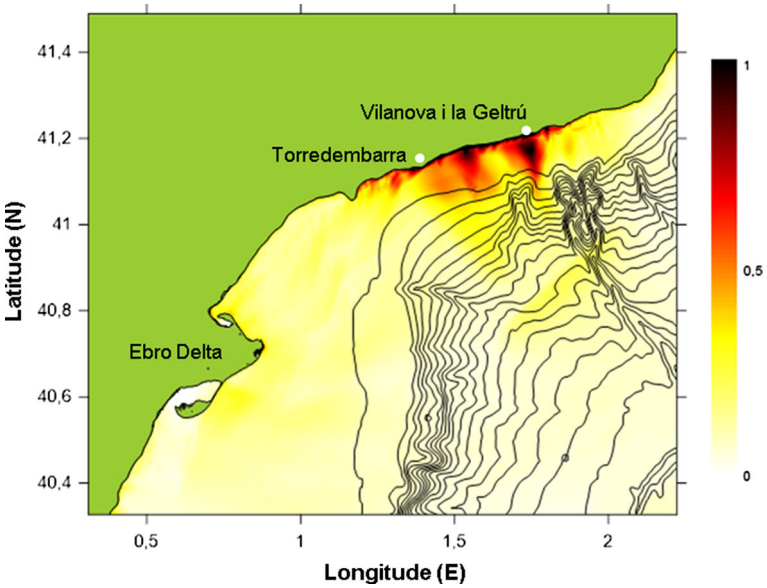

Fig. 9 Maximum water elevation for Salou fault scenario. Bathymetry *contour lines* every 100 m

The maximum FSE in the Ebro Delta produced by the tsunami is plotted in Fig. 10. Wave heights concentrate in Castellon coast and Tortosa Cape. The maximum FSE recorded is 1.5 m and the maximum run-up is 2.29 m. Even though the water elevations obtained are higher close to Castellon, the inundations are larger in the Ebro Delta because of its low-lying topography. Due to its orientation, the northern part of the deltaic coast is less exposed to the tsunami although a wave energy concentration is observed at Sant Jordi Gulf due to the coastline orientation which forces the wave to propagate towards it.

The area flooded by the tsunami triggered in this case is shown in Fig. 10. The trapped wave front is responsible for the complete inundation of Els Alfacs Spit and the barrier beach of El Trabucador (5 km long) and also the flooding of L'Eucaliptus residential area. The total area flooded is about 65 km^2, representing 20% of the total Ebro Delta surface.

4.6 Aggregated scenario

Combining the maximum FSE from all the different computed scenarios in a unique framework provides the aggregated worst-case scenario for any point in the studied area. This map would provide a good approximation for the expected hazard distribution along

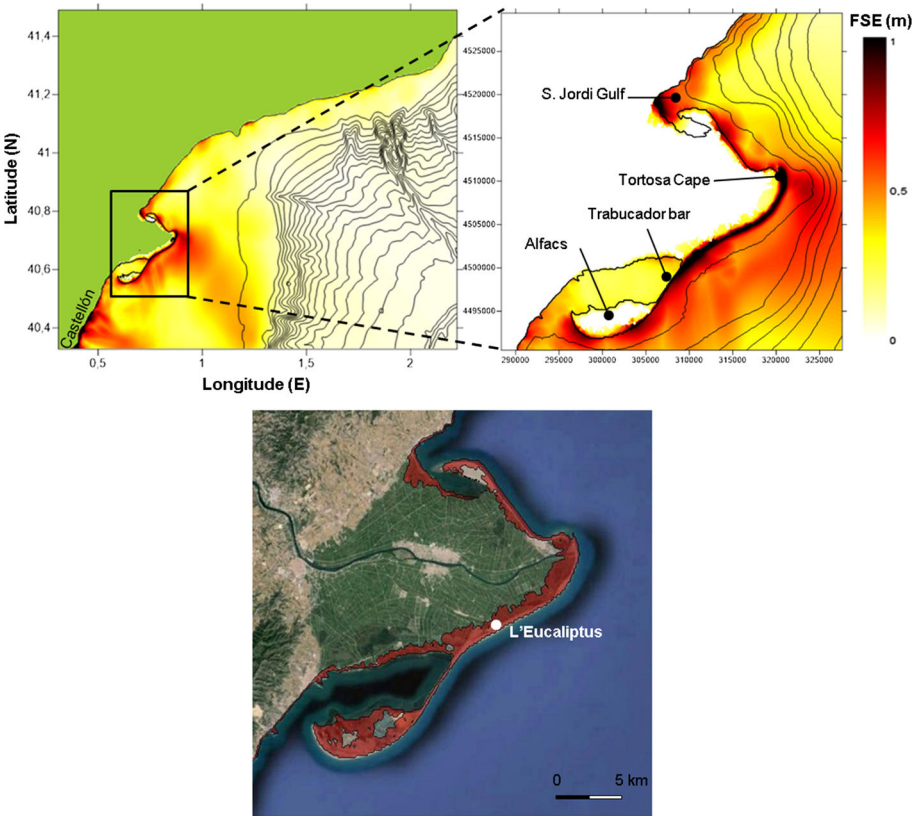

Fig. 10 *Upper panels* Maximum water elevation for the fault of the Amposta basin scenario. Bathymetry *contour lines* every 100 m (*left*) and 20 m (*right*). *Lower panel* Flooded area in *red* for the same scenario in the Ebro Delta area

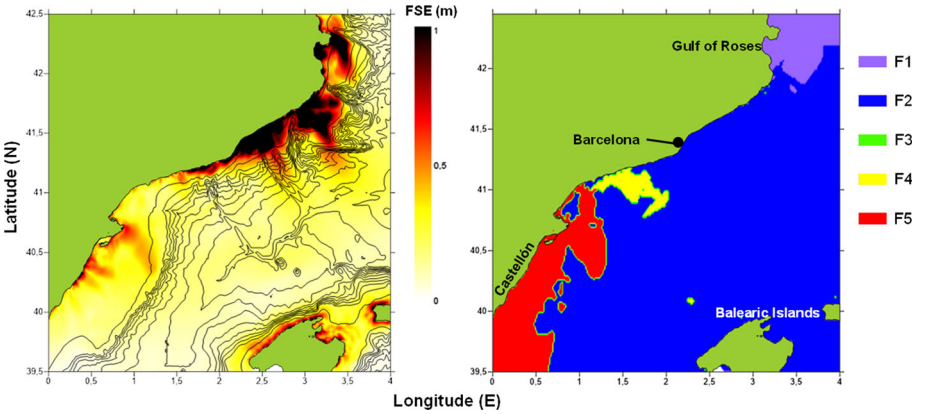

Fig. 11 Combined maximum water elevation (*left*) and fault contribution (*right*) to the aggregated scenario. Bathymetry contour lines every 100 m. *F1* Gulf of Roses; *F2* Blanes, *F3* Barcelona; *F4* Salou; *F5* Amposta basin

the coast, and it would allow identifying areas where the hazard is higher as well as the responsible source. Consequently, these areas can be studied in detail. A joint map with the maximum water elevation from the five different sources and a plot with the fault contribution distribution to the aggregated worst-case scenario are plotted in Fig. 11. The area with the highest hazard associated is the northern half of the Catalan Coast, from the Gulf of Roses to Barcelona, but the hazard is not negligible in the rest of the coastal areas shown in this figure, including Castellón and the Balearic Islands, that are out of the scope of this study. The obtained results suggest that the Barcelona fault is the largest contributor to the aggregated scenario, generating the largest FSEs in more than half of the Catalan Coast. The Gulf of Roses and the Amposta basin faults have also a large contribution, giving the highest FSEs in the areas closest to their location. The Salou fault has local influence too, but it affects the coast with smaller FSEs. On the contrary, the Blanes fault is eclipsed by the Barcelona fault, as it could be expected because both faults are located in nearby areas and the last one has a greater slip. Ultimately, the worst-case tsunami scenario for the Catalan Coast cannot be related to a unique fault since there are four different sources giving rise to the highest FSEs at different stretches of that coast.

5 Summary and conclusions

The Catalan Coast (NW Mediterranean) is an area with a high concentration of population, assets and infrastructures, where the seismic activity is frequent but of low intensity and where the perception of tsunami risk does not exist. Nevertheless, strong earthquakes in the past and the presence of a number of offshore faults in front of this coast suggest that the possibility of having a tsunami in this area, although with a low probability, is not negligible.

Using the numerical model COMCOT and information about the fault features and the WCTSA approach, the worst possible tsunamis that could take place in this region have been simulated, including their generation, propagation and potential impacts on different stretches of the coast.

The results can be considered preliminary, since they are dependent on the assumptions and hypothesis made (summarized as a WCTSA) and could be different if these assumptions were changed. In addition, the accuracy of DTM (0.9 m) is not very favourable for detailed inundation modelling and, therefore, results may change if better topographical data (e.g. LIDAR) were used. However, the presented results are illustrative of the potential hazard posed by tsunamis on large areas of the studied coast.

Results indicate that the worst tsunami scenario is generated by the Barcelona fault, located at the centre of the studied region, in front of the largest city of the studied area and where strategic infrastructures (Barcelona port and airport) are located. The tsunami would flood partially the airport, penetrating 2 km inland and inundating an area of 8.5 km^2. The same tsunami would produce strong currents (up 2 m/s) around the two port mouths and positive and negative FSE of 1 m within the harbour, putting at risk port operations and berthed vessels. Long stretches of the coast would not be flooded due to the existence of high seaside promenades that would protect the beach backside from the waves. This shows the need of a good coastal topography that complements the WCTSA to better explain the hazard distribution.

Other faults could trigger tsunamis affecting other areas of this coast. Thus, the Gulf of Roses fault, located at the northern part of the Catalan Coast, could generate waves penetrating 2.5 km inland and flooding an area of 23.7 km^2 due to the low-lying coast. Similar situation was found in the south of the Catalan Coast, where a tsunami triggered by the Amposta basin fault could flood up to 20% of the Ebro Delta surface.

In addition to discovering the zones most threatened by tsunamis, this study highlighted that the waves would arrive to the coast in few minutes, due to the proximity of the faults to the coastline. Therefore, the available time for warning and evacuation is too short and stresses the need of increasing the awareness of stakeholders and public in general. Consequently, in spite of the low probability of occurrence, the tsunami hazard in the Catalan Coast is significant due to the high level of coastal urbanization that in case of an event would potentially generate large losses. In particular, during the peak tourist season, the large number of assets, campsites and beaches that could be flooded by these events pose a high risk (probability $\times$ loss) of damages and even casualties.

Acknowledgements We would like to express our thanks to HR Wallingford staff, in special to Mr. Lluis Via for his valuable help and Prof. William Allsop, Dr. Ian Chandler and Dr. Aggelos Dimakopoulos for their useful feedback.

References

Alasset PJ, Hébert H, Maouche S, Calbini V, Meghraoui M (2006) The tsunami induced by the 2003 Zemmouri earthquake (MW = 6.9, Algeria): modelling and results. Geophys J Int 166:213–226

Álvarez-Gómez JA, Olabarrieta M, González M, Otero L, Carreño M, Martínez-Solares JM (2010) The impact of tsunamis on the Island of Majorca induced by north Algerian seismic sources. Turk J Earth Sci 19:367–383

Álvarez-Gómez JA, Aniel-Quiroga I, González M, Otero L (2011) Tsunami hazard at the Western Mediterranean Spanish coast from seismic sources. Nat Hazards Earth Syst Sci 11:227–240

Argnani A, Armigliato A, Psgnoni G, Zaniboni F, Tinti S, Bonazzi C (2012) Active tectonics along the submarine slope of south-eastern Sicily and the source of the 11 January 1693 earthquake and tsunami. Nat Hazards Earth Syst Sci 12:1311–1319

Armigliato A, Pagnoni G, Zaniboni F, Tinti, S (2015) Worst-case scenario approach to the tsunami hazard assessment for the coastal areas between Augusta and Siracusa, eastern Sicily, Italy. In: Geophysical

Research Abstracts, Vol. 17, EGU2015-3866. EGU General Assembly 2015, Vienna, Austria. http://meetingorganizer.copernicus.org/EGU2015. Accessed 22 June 2016
BPA, Barcelona Port Authority (2015) Annual Report 2014. http://www.portdebarcelona.cat/en/web/autoritat-portuaria/memoria-vigente. Accessed 22 June 2016
Camfield FE (1982) Calculation of trapped reflected waves. J Waterw Port Coastal Ocean Div Am Soc Civ Eng 108:WW1
Camfield FE (1988) Trapped waves on a wide shelf. In: International conference on natural and man-made hazards in Coastal Zones, Ensenada, Mexico, August 1988
Canals M, Casamor JL, Urgeles R, Farrán M, Calafat AM, Amblas D, Willmott V, Estrada F, Sánchez A, Arnau PJ, Colás S (2004) Mapa del relleu submarí de Calalunya (Seafloor relief map of Catalonia), 1:250 000. Institut Cartogràfic de Catalunya, Barcelona, Spain, 1 map
Chen Q, Kirby JT, Dalrymple RA, Kennedy AB, Chawla A (2000) Boussinesq modeling of wave transformation, breaking and run-up. II: 2D. J Waterw Port Coast Ocean Eng 126:48–56
Chertova MV, Spakman W, Geenen T, van der Berg AP, van Hinsbergen DJJ (2014) Underpinning tectonic reconstructions of the western Mediterranean region with dynamic slab evolution from 3-D numerical modeling. J Geophys Res Solid Earth. doi:10.1002/2014JB011150
Doglioni C, Gueguen E, Harabaglia P, Mongelli F (1999) On the origin of the W-directed subduction zones and applications to the Western Mediterranean. In: Durand B, Jolivet L, Horváth F, Séranne M (eds) The mediterranean basins: tertiary extensions with the Alpine orogen, Special publications, vol 156. Geological Society, London, pp 541–561
El-Sayed A, Romanelli F, Panza GF (2000) Recent seism city and realistic waveforms modeling to reduce the ambiguities about the 1303 seismic activity in Egypt. Tectonophysics 328:341–357
Gailler A, Hébert H, Loevenbruck A, Hernandez B (2013) Simulation systems for tsunami wave propagation forecasting within the French tsunami warning center. Nat Hazards Earth Syst Sci 13:2465–2482
Gaspar-Escribano JM (2004) Cenozoic vertical motions of the Catalan Coastal Ranges (NE Spain): the role of tectonics, isostasy, and surface transport. Tectonics. doi:10.1029/2003TC001511
Geist EL, Parsons T (2006) Probabilistic analysis of tsunami hazards. Nat Hazards 37:277–314
Gelabert B, Sàbat F, Rodríguez-Perea A (2002) A new proposal for the late Cenozoic geodynamic evolution of the western Mediterranean. Terra Nova 14:93–100
Grezio A, Marzocchi W, Sandri L, Gasparini P (2010) A bayesian procedure for probabilistic tsunami hazard assessment. Nat Hazards 53:159–174
Grezio A, Gasparini P, Marzocchi W, Patera A, Tinti S (2012) Tsunami risk assessment in Messina, Sicily—Italy. Nat Hazards Earth Syst Sci 12:151–163
Grilli ST, Taylor OD-S, Baxter DP, Maretzki S (2009) Probabilistic approach for determining submarine landslide tsunami hazard along the upper East Coast of the United States. Mar Geol 261:74–97
Gueguen E, Doglioni C, Fernández M (1998) On the post-25 Ma geodynamic evolution of the western Mediterranean. Tectonophysics 298:259–269
Gutscher MA, Roger J, Baptista MA, Miranda JM, Tinti S (2006) Source of the 1693 Catania earthquake and tsunami (southern Italy): new evidence from tsunami modeling of a locked subduction fault plate. Geophys Res Lett 33:L03809
Hanks TC, Kanamori H (1979) Moment magnitude scale. J Geophys Res 84(B5):2348–2350
Iglesias O, Lastras G, Souto C, Costa S, Canals M (2014) Effects of coastal submarine canyons on tsunami propagation and impact. Mar Geol 350:39–51
Imamura F (1996) Review of tsunami simulation with a finite difference method. In: Yeh H, Liu PL-F, Synolakis C (eds) Long wave runup models. World Scientific Publishing Co, Hackensack, pp 25–42
Jolivet L, Frizon de Lamotte D, Mascle A, Séranne M (1999) The Mediterranean basins: tertiary extension within the Alpine Orogene—an introduction. In: Durand B, Jolivet L, Horváth F, Séranne M (eds) The mediterranean basins: tertiary extensions with the Alpine orogen, Special publications, vol 156. Geological Society, London, pp 1–14
Kennedy AB, Chen Q, Kirby JT, Dalrymple RA (2000) Boussinesq modeling of wave transformation, breaking and run-up. I: 1D. J Waterw Port Coast Ocean Eng 126:39–47
Kherroubi A, Deverchère J, Yelles A, Mercier de Lépinay B, Domzig A, Cattaneo A, Bracène R, Gauliier V, Graindorge D (2009) Recent and active deformation pattern off the easternmost Algerian margin, Western Mediterranean sea: new evidence for contractional tectonic reactivation. Mar Geol 261:17–32
Kim D-H, Lynett P, Socolofosky S (2009) A depth-integrated model for weakly dispersive, turbulent, and rotational fluid flows. Ocean Eng 27:198–214
Lay H, Kanamori H, Ammon CJ, Nettles M, Ward SN, Aster RC, Beck SL, Bilek SL, Brudzinski MR, Butler R, DeShon HR, Ekström G, Satake K, Sipkin S (2005) The great Sumatra-Andaman earthquake of 26 December 2004. Science 308:1127–1133

Liu PL-F, Cho Y-S, Yoon S-B, Seo S-N (1994) Numerical simulations of the 1960 Chilean tsunami propagation and inundation at Hilo, Hawaii. In: El-Sabh MI (ed) Recent developments in tsunami research. Kluwer Academic Publishers, Dordretch, pp 99–115

Liu PL-F, Cho Y-S, Briggs MJ, Kanoglu U, Synolakis CE (1995) Runup of solitary waves on a circular island. J Fluid Mech 302:259–285

Lorito S, Tiberti MM, Basili R, Piatanesi A, Valensise G (2008) Earthquake-generated tsunamis in the Mediterranean Sea: scenarios of potential threats to southern Italy. J Geophys Res 113:B01301. doi:10.1029/2007JB004943

Lynett P, Liu PL-F (2002) A numerical study of submarine landslide generated waves and runup. Proc R Soc A 458:2885–2910

Lynett P, Liu PL-F (2004) A two-layer approach to water wave modeling. Proc R Soc A 460:2637–2669

Lynett P, Wu T-R, Liu PL-F (2002) Modeling wave runup with depth-integrated equations. Coast Eng 46:89–107

Malinverno A, Ryan W (1986) Extension in the Tyrrhenian sea and shortening in the Appennines as result of the migration driven by sinking of the lithosphere. Tectonics 5:227–245

Mansinha L, Smylie DE (1971) The displacement fields of inclined faults. Bull Seismol Soc Am 61:1433–1440

Masana E, Villamarín JA, Sánchez-Cabañero JG et al (2001a) Seismogenic faulting in an area of low seismic activity: paleoseismicity of the El Camp fault (northeast Spain). Nors J Geosci 80:229–241

Masana E, Villamarín JA, Santanach P (2001b) Paleoseismic results from multiple trenching analysis along a silent fault: the El Camp fault (Tarragona, northeastern Iberian Peninsula). Acta Geol Hispánica 36:329–354

Okada Y (1985) Surface deformation due to shear and tensile faults in a half space. Bull Seismol Soc Am 75:1135–1154

Okal E, Synolakis CE (2008) Far-field tsunami hazard from mega-thrust earthquakes in the Indian Ocean. Geopys J Int 172:995–1015

Olivera C, Susagna T, Roca A, Goula X (1992) Seismicity of the Valencia trough and surrounding areas. Tectonophysics 203:99–109

Olivera C, Redondo E, Lambert J et al (2006) Els terratremols dels segles XIV i XV a Catalunya. Institut Cartogràfic de Catalunya, Barcelona

Pagnoni G, Armigliato A, Tinti S (2015) Scenario-based assessment of buildings damage and population exposure due to earthquake-induced tsunamis for the town of Alexandria, Egypt. Nat Hazards Earth Syst Sci 15(12):2669–2695. doi:10.5194/nhess-15-2669-2015

Papadopoulos, G.A. (2016) Chapter 7—Tsunami Early Warning Systems and Risk Mitigation. In: Papadopoulos, G.A. (ed) Tsunamis in the European-Mediterranean Region, Elsevier, Boston, 2016, Pages 179-226, ISBN 9780124202245, http://dx.doi.org/10.1016/B978-0-12-420224-5.00007-7

Papadopoulos GA, Gracia E, Urgeles R, Sallares V, De Martini PM, Pantosti D, Gonzalez M, Yalciner AC, Mascle J, Sakellariou D, Salamon A, Tinti S, Karastathis V, Fokaefs A, Camerlenghi A, Novikova T, Papageorgiou A (2014) Historical and pre-historical tsunamis in the Mediterranean and its connected seas: geological signatures, generation mechanisms and coastal impacts. Mar Geol 354:81e109. doi:10.1016/j.margeo.2014.04.014

Pelinovsky E, Kharif C, Riabov I, Francius M (2002) Modelling of tsunami propagation in the vicinity of the French coast of the Mediterranean. Nat Hazards 25:135–159

Perea H (2009) The Catalan seismic crisis (1427 and 1428; NE Iberian Peninsula): geological sources and earthquake triggering. J Geodyn 47:259–270

Perea H, Figueiredo PM, Carner J, Gambini S, Boydell K (2003) Paleoseismological data from a new trench across the El Camp Fault (Catalan Coastal Ranges, NE Iberian Peninsula). Ann Geophys 46:763–774

Perea H, Masana E, Santanach P (2006) A pragmatic approach to seismic parameters in a region with low seismicity: the Case of Eastern Iberia. Nat Hazards 39:451–477

Perea H, Masana E, Santanach P (2012) An active zone characterized by slow normal faults, the northwestern margin of the València trough (NE Iberia): a review. J Iber Geol 38:31–52

Piatanesi A, Tinti S (1998) A revision of the 1693 eastern Sicily earthquake and tsunami. J Geophys Res 103(B2):2749–2758

Piatanesi A, Tinti S (2002) Numerical modeling of the September 8, 1905 Calabrian (southern Italy) tsunami. Geophys J In 150:271–284

Roca E (1996) La evolución geodinámica de la Cuenca Catalano-Balear y áreas adyacentes desde el Mesozoico hasta la actualidad. Acta Geol Hispánica 29:3–25

Roca E (2001) The northwestern-mediterranean basin (Valencia trough, Gulf of Lions and Liguro-Provençal basins): Structure and geodynamic evolution. In: Ziegler PA, Cavazza W, Robertson AHF, Crasquin-Soleau S (eds) Peri-Tethys memoir, IGCP 369: Peri-Tethyan rift/wrench basins and passive margins.

Mémoires du museum national d'histoire naturelle, vol 186. Commission for the Geological map of the world, Paris, pp 671–706
Roca E, Guimerà J (1992) The Neogene structure of the eastern Iberian margin: structural constrains on the crustal evolution of the Valencia trough (western Mediterranean). Tectonophysics 203:203–218
Roca E, Sans M, Cabrera L, Marzo M (1999) Oligocene to Middle Miocene evolution of the central Catalan margin (northwestern Mediterranean). Tectonophysics 315:209–233
Roger J, Hébert H (2008) The 1856 Djijelli (Algeria) earthquake and tsunami: source parameters and implications for tsunami hazard in the Balearic Islands. Nat Hazards Earth Syst Sci 8:721–731
Rosenbaum G, Lister GS, Duboz C (2002) Reconstruction of the tectonic evolution of the western Mediterranean since the Oligocene. J Virtual Explor 8:107–130
Royden LH (1993) Evolution of the retreating subduction boundaries formed during continental collision. Tectonics 12:629–638
Sàbat F, Roca E, Muñoz JA et al (1996) Role of extension and compression in the evolution of the eastern margin of Iberia: the ESCI-Valencia Trough seismic profile. Rev Soc Geol España 8:431–448
Scheer SJ, Varela V, Eftychidis G (2012) A generic framework for tsunami evacuation planning. Phys. Chem. Earth, Parts A/B/C 49:79–91
Scotti O, Baumont D, Quenet G, Levret A (2004) The French microseismic database SISFRANCE—objectives, results and perspectives. Ann Geophys 47:571–581
Shore Protection Manual (SPM) (1984) Coastal engineering research centre, waterways experiment station. US Army Corps of Engineers, Vicksburg Miss
Soloviev SL, Solovieva ON, Go CN, Kim KS, Shchetnikov NA (2000) Tsunamis in the Mediterranean Sea: 2000 B.C.—2000 A.D. Kluwer Academic Publishers, Dordretch, p 237
Tinti S, Piatanesi A (1996) Numerical simulations of the tsunami induced by the 1627 earthquake affecting Gargano, southern Italy. J Geodyn 21:141–160
Tinti S, Armigliato A, Pagnoni G, Zaniboni F (2005a) Scenarios of giant tsunamis of tectonic origin in the Mediterranean. ISET J Earthq Technol 42:171–188
Tinti S, Armigliato A, Tonini R, Maramai A, Graziani L (2005b) Assessing the hazard related to tsunamis of tectonic origin: a hybrid statistical-deterministic method applied to southern Italy coasts. ISET J Earthq Technol 42:189–201
Tinti S, Pagnoni G, Zaniboni F (2006) The landslides and tsunamis of the 30th of December 2002 in Stromboli analysed through numerical simulations. Bull Volcanol 68:462–479
Titov VV, Sinolakis CE (1998) Numerical modeling of tidal wave run-up. J Waterw Port Coast Ocean Eng 124:157–171
Titov VV, González FI, Bernard EN, Eble MC, Mofjeld HO, Newman JC, Venturato AJ (2005) Real-time tsunami forecasting: challenges and solutions. Nat Hazards 35:41–58
Tonini R, Armigliato A, Pagnoni G, Zaniboni F, Tinti S (2011) Tsunami hazard for the city of Catania, eastern Sicily, Italy, assessed by means of worst-case credible tsunami scenario analysis (WCTSA). Nat Hazards Earth Syst Sci 11:1217–1232
UNESCO-IOC (2009) Tsunami risk assessment and mitigation for the Indian Ocean, knowing your tsunami risk—and what to do About It. UNESCO—Intergovernmental Oceanographic Commission (IOC), Manuals and Guides 52, 2009
van Hinsbergen DJJ, Vissers RLM, Spakman W (2014) Origin and consequences of western Mediterranean subduction, rollback, and slab segmentation. Tectonics 33:393–419
Vergés J, Sàbat F (1999) Constraints on the neogene Mediterranean kinematics evolution along a 1000 km transect from Iberia to Africa. In: Durand B, Jolivet L, Horváth F, Séranne M (eds) The mediterranean basins: tertiary extensions with the Alpine orogen, Special publications, vol 156. Geological Society, London, pp 63–80
Wang X, Liu PL-F (2005) A numerical investigation of Bourmedes-Zemmouri (Algeria) earthquake and tsunami. Comput Model Eng Sci 10:171–184
Wang X, Liu PL-F (2006) An analysis of 2004 Sumatra earthquake fault plane mechanisms and Indian Ocean tsunami. J Hydraul Res 44:147–154
Wei G, Kirby JT (1995) Time dependent numerical code for extended Boussinesq equations. J Waterw Port Coast Ocean Eng 12:251–261
Wells DL, Coppersmith KJ (1994) New empirical relationships among magnitude, rupture length, rupture width, rupture area, and surface displacement. Bull Seism Soc Am 84(4):974–1002
Yelles Chaouche A, Roger J, Déverchère J, Bracène R, Domzig A, Hébert H, Kherroubi A (2009) The 1856 tsunami of Djidjelli (Eastern Algeria): seismotectonics, modelling and hazard implications for the Algerian coast. Pure appl Geophys 166:283–300